Shadow imaging: attenuation projection of acoustic waves from a circular array without arrival picking

David C. Henley

ABSTRACT

Seismic physical modeling systems can be used to record acoustic and elastic wavefields for a wide variety of targets and acquisition geometries of interest not only to seismologists, but to engineering and medical professionals, as well. We demonstrate here a novel processing scheme for the transmitted acoustic amplitudes measured by a circular array of ultrasonic receiver transducers coincident with a circular array of ultrasonic source transducers, immersed in the water tank of the modeling system.

Most processing techniques for transmitted acoustic waves require ‘picking’ the acoustic ‘arrivals’ for a ‘time of flight’ for the acoustic energy transmitted along the assumed raypaths for the energy. A variety of techniques, usually referred to as ‘tomography’, can be applied to provide a low-resolution image of any object(s) immersed within the circular arrays of the acquisition system. Since most tomographic methods rely on discrete arrival times of the acoustic wavefronts, they provide a ‘delay time’ or time-of-flight’ image of any immersed object(s), but they are very sensitive to errors in the time picks.

We demonstrate here, instead, a form of tomographic imaging which does not need explicit time picks of acoustic wave arrivals, but instead uses much less sensitive acoustic wave envelope amplitudes chosen at geometrically consistent points on each measured acoustic record. These envelope amplitudes depend inversely upon the attenuation along each transmission path. Hence we term our technique ‘shadow imaging’, since it orients the attenuation ‘shadow’ observed from each source around the array, then stacks the oriented shadows to form an attenuation image (a form of projection tomography), which we hope to use as a low order starting model for Full Waveform Inversion.

INTRODUCTION

Ultrasonic modeling systems are becoming popular for studying the acoustic or elastic wave response of scale models which emulate various types of geological structures encountered by seismologists (Wong et al, 2010; Romahn and Innanen, 2017; Wong et al, 2019). Because the properties and shapes of the components of the physical model can be controlled by the modeler, as well as the locations of the ultrasonic transducers used to probe the model, most events on the trace ensembles created during a modeling run can be identified as specific wave modes. This, in turn, provides guidance for enhancing the desired modes (like reflections) and attenuating the undesired ones (direct arrivals, refractions, multiples, converted waves, for example). Secondarily, physical modeling data can be used to confirm data created by various numerical modeling programs (Henley and Wong, 2019; Henley, 2020). This can be important when developing various Full Waveform Inversion methods for seismic data, since most of these techniques rely on minimizing the differences between a processed seismic data image and an image created by a forward modeling scheme from an incrementally updated numerical velocity/density model.

Studying and confirming conventional seismic reflection data imaging processes is not the only use for a physical modeling system; in our present study, we study a situation more similar to medical ultrasonic imaging, than to any current seismic probing method. Instead of immersing a geological analog model in water in the modeling tank and surveying it with arrays of ultrasonic sources and receivers to simulate seismic trace ensembles, we introduce two ultrasonic piezopin transducers, at a constant common depth, into the modeling tank. We then position the source transducer sequentially at one of 35 positions around the circumference of a horizontal circle. For each position of the source transducer, we record signals into the receiver transducer at each of 72 positions around the same circle on which the source is positioned. Because of the potential physical interference of the jigs which position the transducers, roughly half of the potential 2520 raypaths across the circular arrays cannot be achieved. Nevertheless, 1331 clear transmission raypaths can be achieved, and we can record 35 trace ensembles, one per source position, corresponding to a source recorded by a circular array with the source on the perimeter of the circle (Wong et al, 2020). Figure 1a shows a schematic of the concentric circular arrays, while Figure 1b shows the possible raypaths between source points and receiver points, before eliminating those rendered impossible by physical limitations of the transducer positioning apparatus. Figure 2 illustrates a few typical source gathers recorded by the physical modeling system into the circular array with no target present within the array.

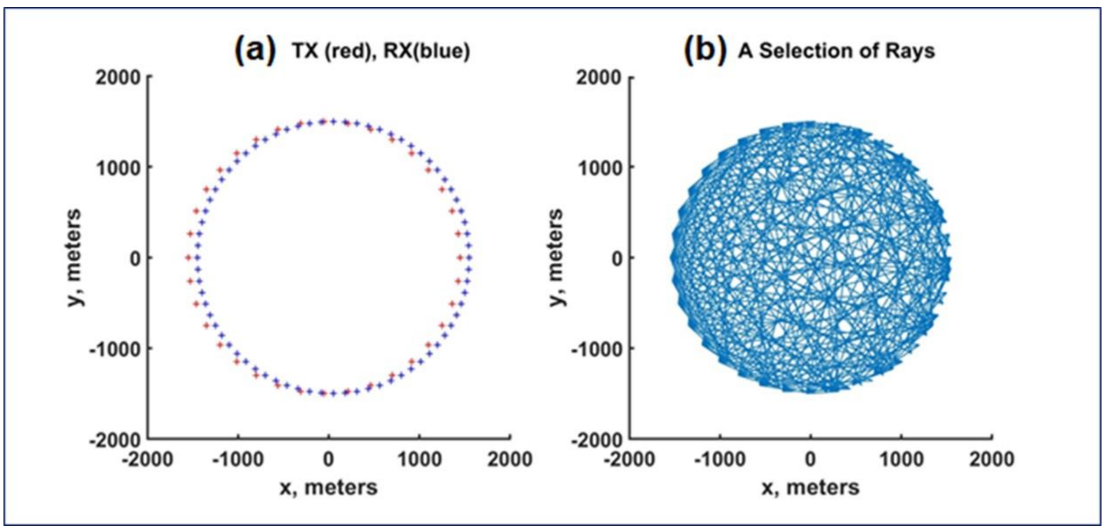

FIG. 1. a). Schematic of the concentric source (red) and receiver (blue) transducer arrays for the ultrasonic modeling apparatus. Distances shown are the scaled distances. b) Possible raypaths between source points and receiver points, without considering physical constraints due to the transducer fixtures.

The physical modeling setup described above is designed primarily to observe direct transmitted acoustic waves through the water medium; which is all that will be observed (other than artifacts from the modeling system) in the absence of objects inside the circle of the transducer arrays (see Figure 2). If, however, we place an object inside the acquisition circle, we expect to disrupt the direct arrival waves and to create other wave modes (backscatter and diffractions). For the present, we disregard diffractions and backscatter and focus on the direct arrival waves. Our objective in this study is to analyze the differences between data from an empty array and an array containing an object, to obtain a low-resolution image of the intruding object. This suggests a tomographic method, and we have pursued two different approaches which are related to the two commonly used types of tomography: ‘time-of-flight’ or velocity tomography, based on arrival time picks, and ‘attenuation’ tomography, based on arrival amplitudes.

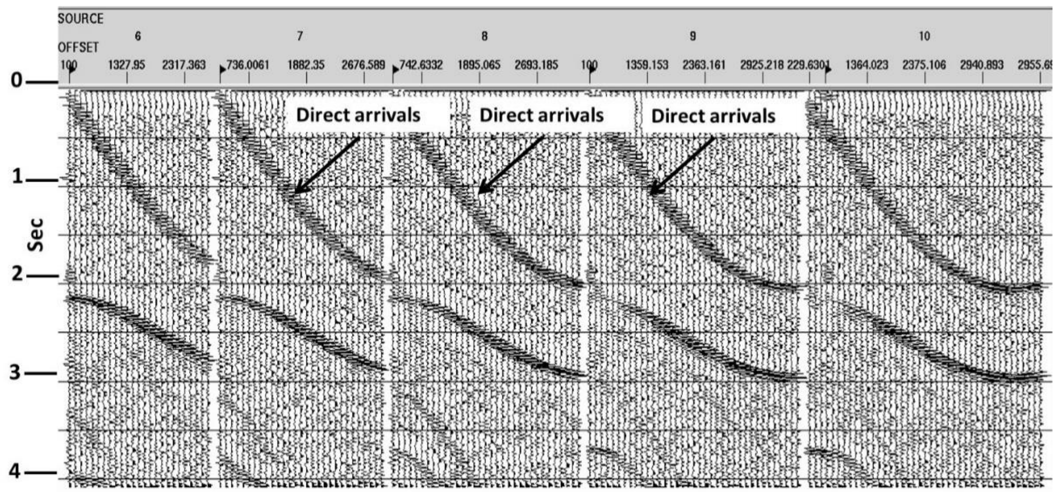

FIG. 2. Typical source gathers for the 1500m radius circular array, with no target objects inside the array. The direct arrival events are our primary focus, all other events are artifacts of the acquisition apparatus or wave modes of secondary interest. Times and distances are scaled to seismic scale.

Time of flight approach

In a previous study (Henley, 2021), we developed a technique based on travel time picks, and thus related to conventional velocity tomography. In this method, we compared the first arrival times picked from the data generated with the array space empty (the null experiment) to those picked from the data generated with an object inside the array circle. Since the data sets have source gathers with corresponding geometry, we can compare the traces with common source-receiver coordinates. Those traces showing arrival time differences are assumed to represent raypaths intercepting an object located within the circular array; those showing no arrival time differences are assumed to represent raypaths within the water medium which do not intercept an object. For each source gather of traces, sorted by source-receiver azimuth, we flag the first and last traces with arrival time differences. These traces, then, are the edges of a shadow cast by the object on the receiver array.

With the edges of shadows flagged on each source gather, we then create artificial “shadows” within each source gather by zeroing all trace samples except those within the boundaries of each shadow, which we set to a constant value, tapered at the beginning and end of traces. Thus, we have source gathers for the circular array containing artificial “shadows” created from the edges of arrival time pick anomalies.

To form an image from these shadow gathers, they must be oriented and rotated to a common reference frame, using the known coordinates of the sources and receivers in the circular array. As created, the shadows in the shadow gather are oriented vertically in each gather, where the vertical coordinate is transit time, relative to the picked arrival time, and the horizontal coordinate is source-receiver azimuth. Each source gather can be considered to be an angular scan, between two source-receiver azimuths, of the space, and any included objects, within the array of receivers accessible from that source. To appropriately rotate the shadows within the gathers to their proper orientation relative to the acquisition circle, each must be tilted, relative to its centre, by an amount determined by the position of its source on the circular array.

We adapted the linear moveout operation to apply rotation to each source gather. First, we applied an initial tilt to all the shadows by applying the Radial Trace dip transform (Henley, 1999, 2003) to each source gather, using a fixed dip parameter, and a set of source-receiver offsets derived from the source-receiver offsets of each source gather. We then assigned new source-receiver offset values to the traces in the RT-transformed source gathers, where these offset values were computed from the azimuth of the source relative to the centre of the array, scaled by the radius of the array. A set of linear moveout functions was then created, one for each source, such that application of the linear moveout function rotated each shadow, by applying shifts to the individual traces proportional to their computed ‘offset’ values. The parameters were adjusted to yield one complete shadow rotation over the group of 35 source gathers. The rotated shadow gathers were then stacked to yield an image.

One problem with this approach is the uncertainty introduced into the image space by the failure to properly convert vertical coordinates of arrival time to depth, and to gracefully convert both to common image coordinates (Henley, 2021). A second significant problem is the reliance on picked arrival times, which are always subject to error, especially in the presence of noise. Hence, we decided to explore the alternate tomographic approach of attenuation imaging.

Attenuation approach

The time-of-flight or velocity image tomographic approach requires only a single value from the trace representing each raypath—the first arrival time of the wavelet representing the energy packet transmitted from source to receiver. Choosing this arrival time is always a non-linear process, which assumes that the energy packet is infinitely resolved (has infinite bandwidth), and hence has a single discreet arrival time. The arrival time picking process is thus susceptible to several factors, including the actual bandwidth of the energy packet, the phase of the wavelet, and any interfering noise. To partially avoid these vulnerabilities, we consider utilizing a broader, less susceptible attribute of the transmitted energy packet—its envelope amplitude, or magnitude. Our assumption here is that the reciprocal magnitude, when scaled for spherical spreading over the transmission distance will be a sensitive measure of attenuation due to objects in the raypath. If we create shadows from the attenuation values, they will be scaled by the degree of attenuation in the raypaths, instead of being simple ‘black or white’ shadows as created for the previous transit time imaging (Henley, 2021). As in the previous approach, we still consider the raypaths to be straight from source to receiver, and hence a ‘zero order’ projection approach is implied.

As before, our source gather data, after being transformed to attenuation values, require transformation to the image domain, including rotation and proper orientation relative to each other. This time, however, we transform the data in such a way that the coordinates are related immediately to the cartesian coordinates of the image domain. In the next section, we describe the processing operations used to extract attenuation information from the raw data ensembles and form a projection shadow image which may act as a low-resolution starting model for subsequent full-waveform inversion.

METHOD

Arrival alignment

For the particular experimental setup we used for acquiring circular array data, we recorded two sets of data, one with no targets within the circular aperture of the array (the ‘null’ data set), and one with a target present inside the array (the ‘target’ data set). Since we know the exact coordinates of source and receiver transducers, and hence their source-receiver offset distances, as well as the exact velocity of the medium (water), we can compute the straight-ray transit time for acoustic energy transmitted from any source point to any receiver point. We apply these transit times as static shifts to all the traces in both data sets to align the arrival wavelets at an arbitrarily chosen zero time. To refine this alignment, we apply a trim statics operation, using the entire data set for each of the two surveys to provide the model wavelet for the trim statics.

To finalize the aligned data sets for analysis, we apply Gabor deconvolution (Margrave et al, 2011), followed by a broadband zero-phase filter to regularize the arrival waveforms and make their phases consistent. The overall amplitudes are adjusted by removing geometric spreading, using the known source-receiver distances. Example source gathers are shown in Figure 3 for the null data set, while corresponding gathers for the target data set are shown in Figure 4. Note that in both cases, the zero time of the arrivals has been set to 120ms to buffer the traces for analysis. The arrival times of all the waveforms are as if the source were centered at zero, and all the receivers were placed at a uniform radius around the source.

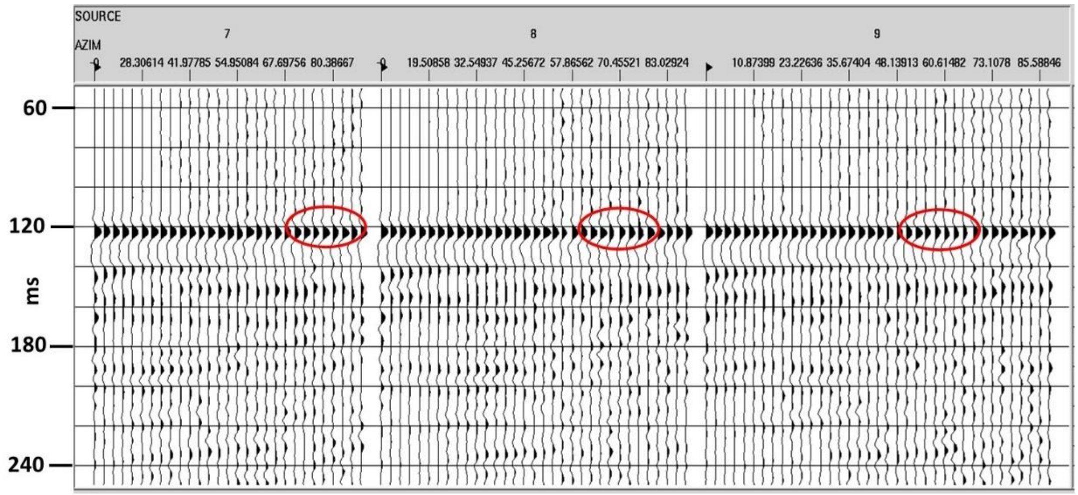

FIG.3. Typical source gathers from the 'null' data set with no target within the circular array. Arrivals have been flattened by the water travel time across the circular array, adjusted by trim statics, phase-adjusted by Gabor deconvolution, bandlimited, adjusted for spherical spreading, and aligned at 120ms. Red ovals indicate likely shadow zones for a target (see Figure 4).

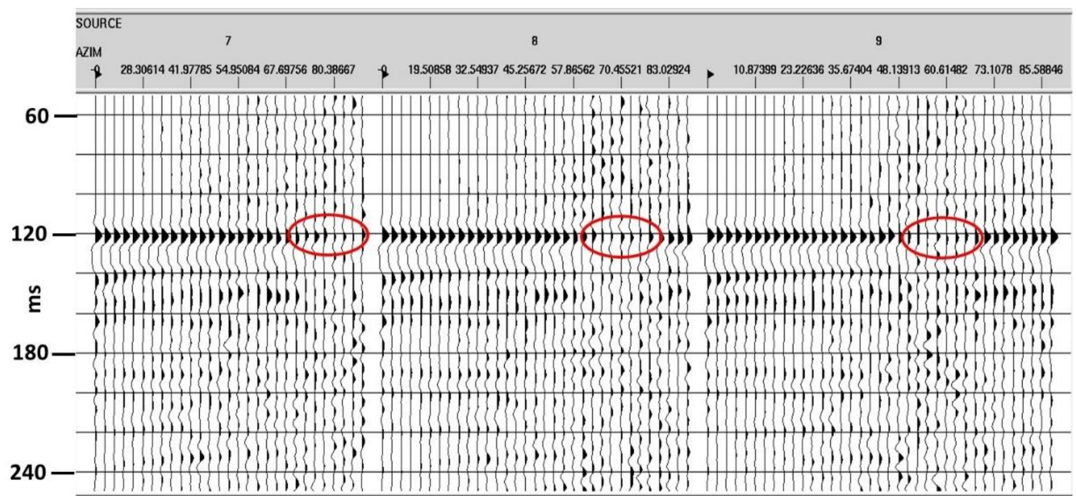

FIG.4. Typical source gathers from the 'target' data set with an unknown target within the circular array. Arrivals have been flattened by the water travel time across the circular array, adjusted by trim statics, phase-adjusted by Gabor deconvolution, bandlimited, adjusted for spherical spreading, and aligned at 120ms. Note the amplitude dimming in the likely target zones (red ovals).

Attenuation

One approach to obtaining attenuation values would be to subtract the null data set amplitudes, prepared as described above, from the corresponding amplitudes of the target data set. We decided instead, however, to construct a new data set, using only the target data, consisting of traces whose sample values would represent the magnitude of an acoustic energy packet traversing the path between source and receiver for a particular source and receiver. The length of these traces is set to a value greater than the transit time across the whole circular array. The constant amplitude value assigned to each trace represents transmissivity for the raypath, or magnitude of the transmitted acoustic energy represented by the source and receiver for that trace, and is assigned as follows:

- The perigram (envelope function) is computed for each trace and smoothed in time.

- The transit time of the average perigram maximum is chosen (125ms, in this case), and the perigram value at that time for each trace is extracted to a trace header.

- For each trace, the amplitude values are scaled by to the reciprocal of the stored trace header, to form 'attenuation' traces.

- Each trace is smoothed over the entire trace length, in effect yielding a constant value representative of the attenuation experienced by acoustic energy traversing the raypath represented by the trace.

Figure 5 shows five source gathers from the target data set, with the amplitude values replaced by their smoothed envelope values (perigrams). Plotted at the top are the trace values extracted at 125ms, the nominal maximum value for the arrival envelopes. When the traces are normalized by the reciprocal max amplitudes, they appear as in Figure 6; and when they are smoothed over the entire trace length, they are as shown in Figures 7 and 7a, where the attenuation trace gathers are displayed as a function of source-receiver azimuth. Each trace represents the total attenuation experienced by an acoustic energy pulse travelling from a specific source point along a constant-angle raypath to the receiver array.

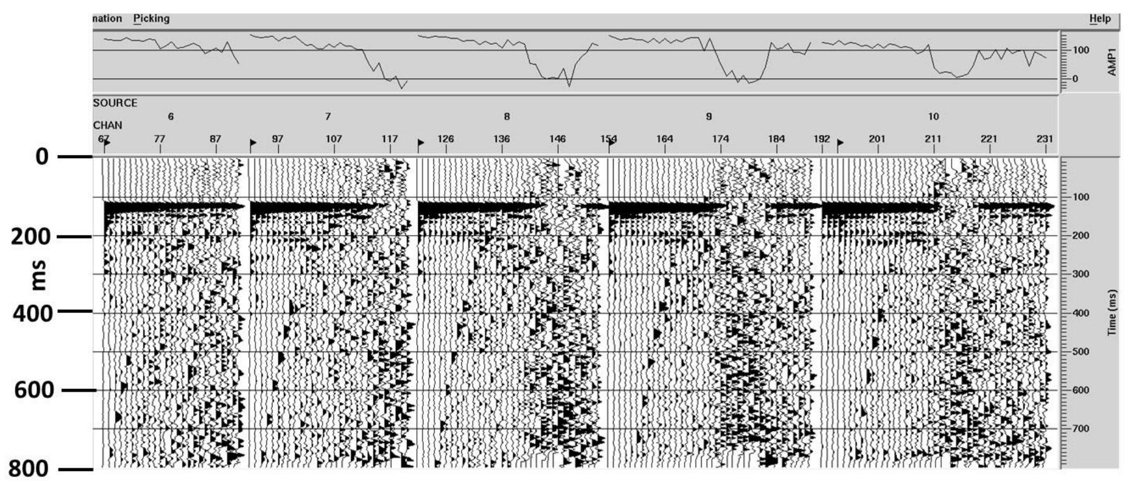

FIG. 5. Five source gathers, first arrivals aligned at 120ms, Gabor deconvolution, spherical spreading, perigrams (wavelet envelope or magnitude) computed and smoothed in time. Perigram value at 125ms (nominal maximum) plotted along the top of each gather.

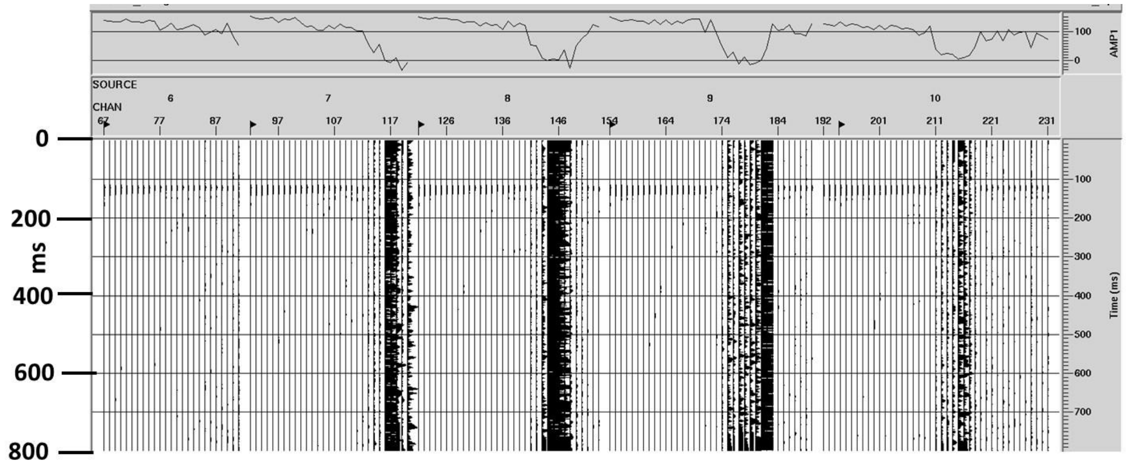

FIG. 6. Five source gathers, as in Figure 5, but normalized by the perigram value at 125ms. Perigram value at 125ms plotted along the top of each gather.

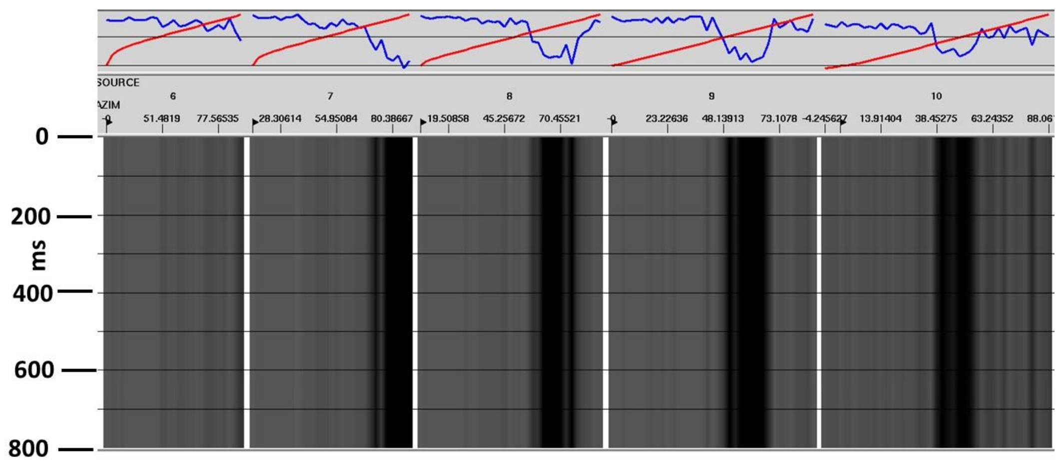

FIG. 7. Source gathers from Figure 6, trace amplitudes are the projected maximum perigram value for each trace, representing the attenuation experienced by energy traveling along the travel path represented by the trace. Shadow intensity as a function of source-receiver azimuth.

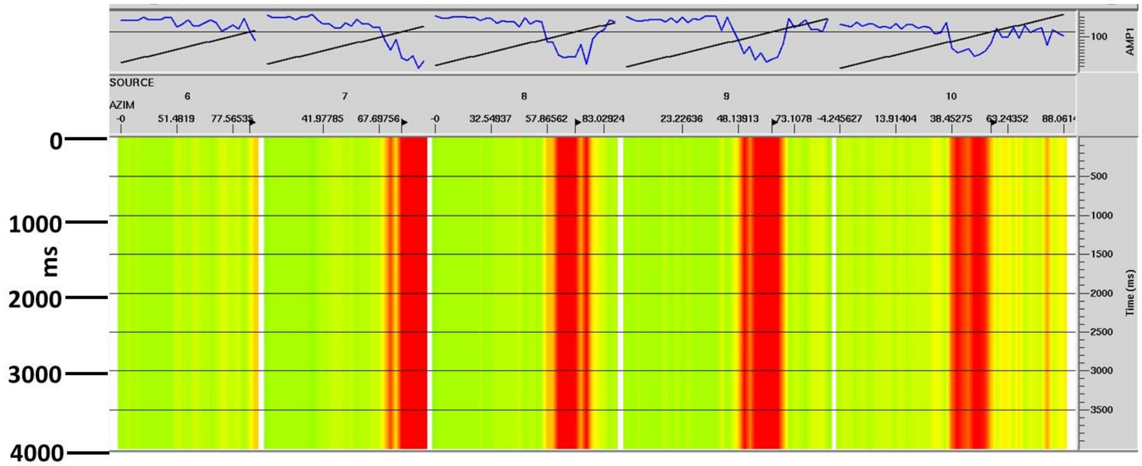

FIG. 7a. Source gathers showing shadow intensity as a function of source-receiver azimuth on extended traces

The coordinates of the trace ensembles in Figures 7 and 7a are raypath parameter (slope, or azimuth) and travel time, similar to the coordinates assumed by the traces created with the Radial Trace Transform, a simple re-mapping of seismic data from the conventional source-receiver offset (X) vs travel time (T) domain to the domain of ray parameter vs travel time. Based on this similarity, we chose to apply an inverse Radial Trace Transform (Henley, 2003; Henley, 1999) to each of the 35 source gathers to transform them from attenuation as a function of source-receiver azimuth and time to attenuation as a function of source-receiver offset (in this case, an artificial parameter) and time. A schematic showing this data re-mapping is shown in Figure 8. Figure 9 displays some of the transformed gathers, which now look more like conventional source gathers, except that the ‘offset’ parameter displayed along the horizontal axis is not a true source-receiver offset, but an artificial parameter representing the separation of source and receiver in cartesian image space. These ensembles represent the total attenuation along any raypath within the aperture of a given source. The final preparation of these source gathers is to convert the travel time coordinate to depth Figure 9a), using the nominal water velocity. This results in attenuation trace gathers which can be rotated and shifted relative to each other in the same coordinate system, before being stacked to yield ‘shadow’ or attenuation images of the interior of the circular acquisition array.

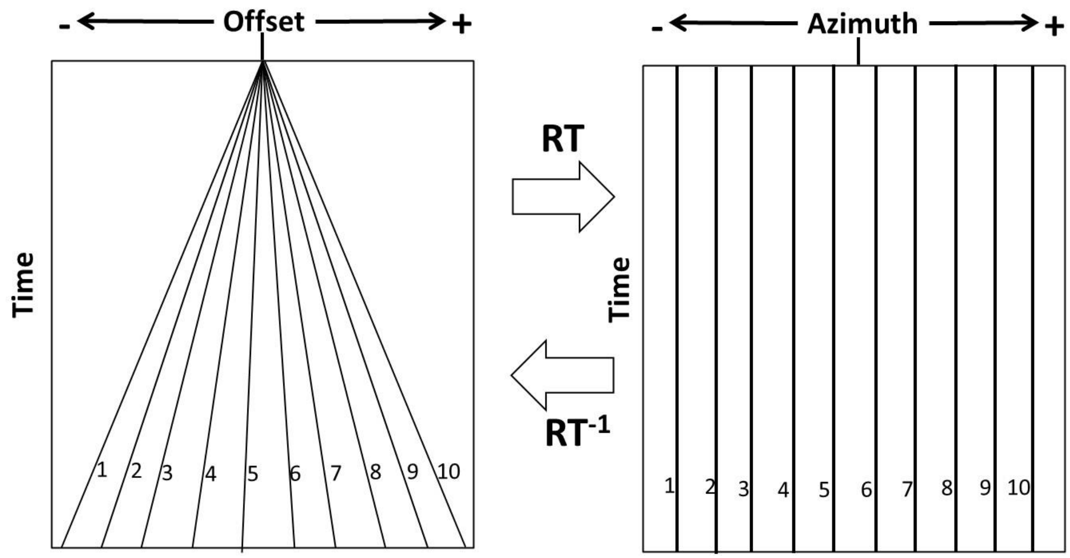

FIG. 8. Schematic showing the mapping between the X-T domain and the Azimuth-T domain induced by the radial trace (RT) transform. Numbered traces in the X-T domain with particular slopes (ray parameters) map to vertical traces in the azimuth-T domain, as shown. Hence, the inverse RT transform maps a source gather sorted by azimuth/travel time (Figures 7 and 8) to source beam gathers sorted by 'source-receiver offset' (a fictitious parameter) and travel time (Figure 9).

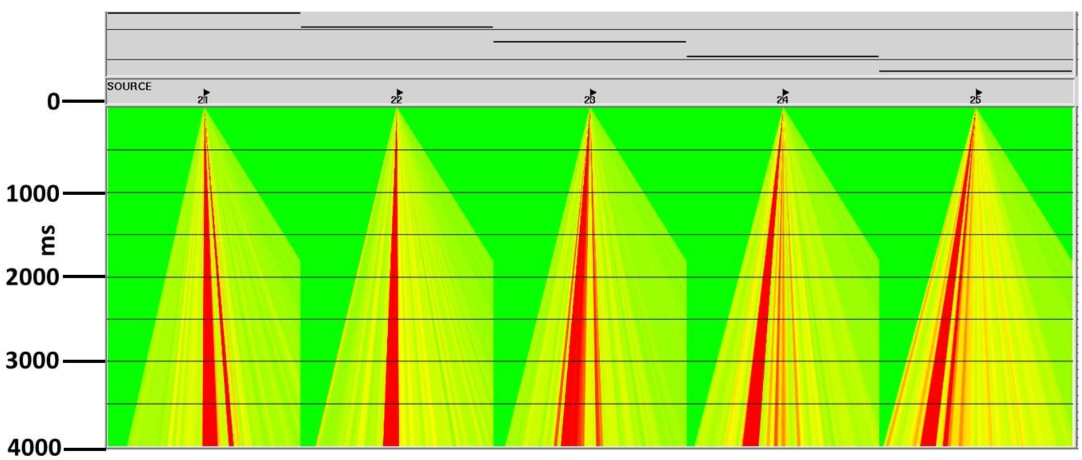

FIG. 9. Typical source beam gathers after inverse RT transform from ray-parameter vs. transit time to 'source-receiver offset' vs. transit time. Offset in this case is an artificial parameter, chosen to properly scale the beam gathers.

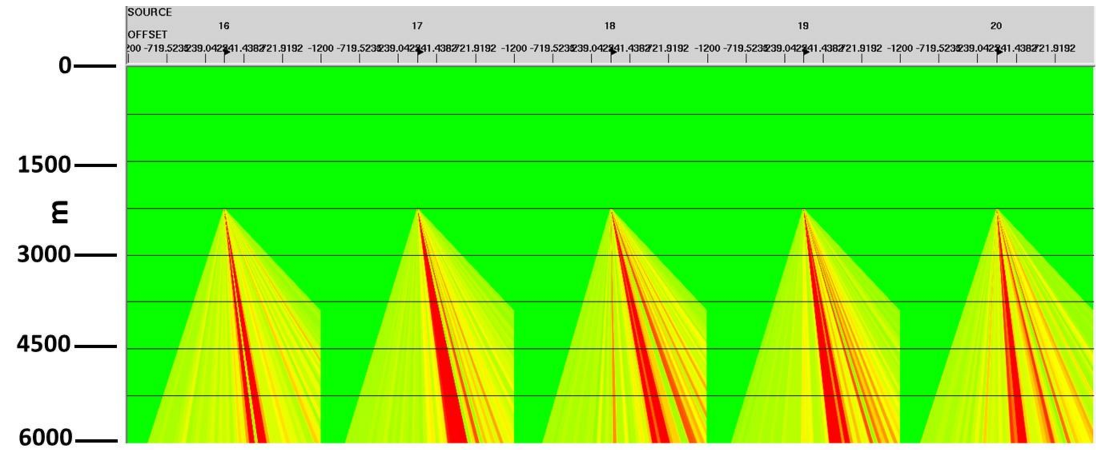

FIG. 9a. source beam gathers converted to depth.

Manipulating source shadow gathers

To prepare source image gathers for being stacked into a common image space, one of the more obvious steps is to position the source points of the individual gathers at their proper locations around the circumference of the image circle, based on their source number, as shown in Figure 10. It is then obvious that the shadow beams within the individual gathers need to be rotated to impinge on the image space at their proper orientation. One of the available parameters to affect this rotation is the artificial source-receiver offset parameter in the trace headers of all the source shadow gathers. Applying a linear constant to this parameter effectively tilts, or 'rotates' the beams or shadows within each gather, as illustrated in Figure 11 for a small group of gathers. Changing the value of the constant for each gather effectively determines the degree of tilt or rotation applied within the gather. Hence, we can develop formulas for positioning and orienting source shadow gathers, using source number, source azimuth, source-receiver offset, and source-receiver azimuth as independent variables.

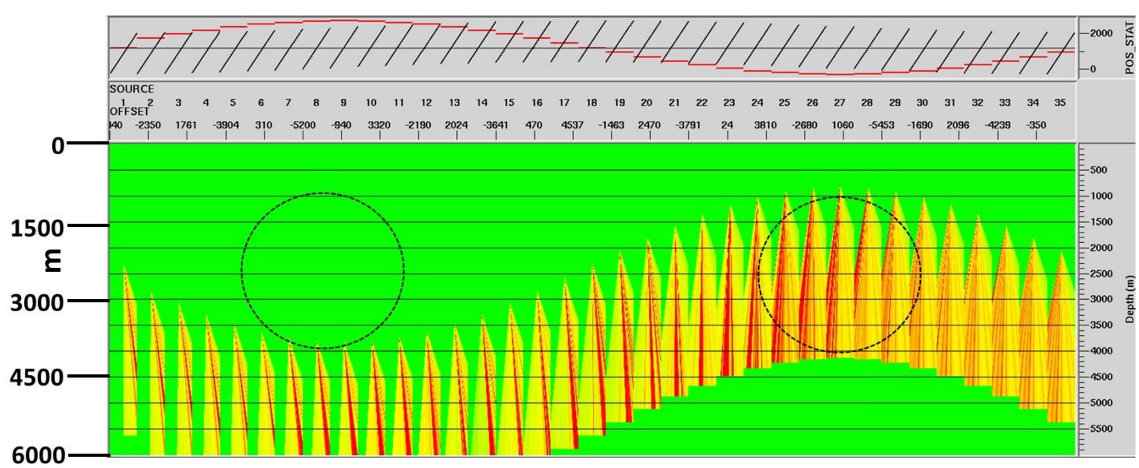

FIG. 10. Source beam gathers with origins posted at source positions around the acquisition circle. Black circles indicate relative size of acquisition array.

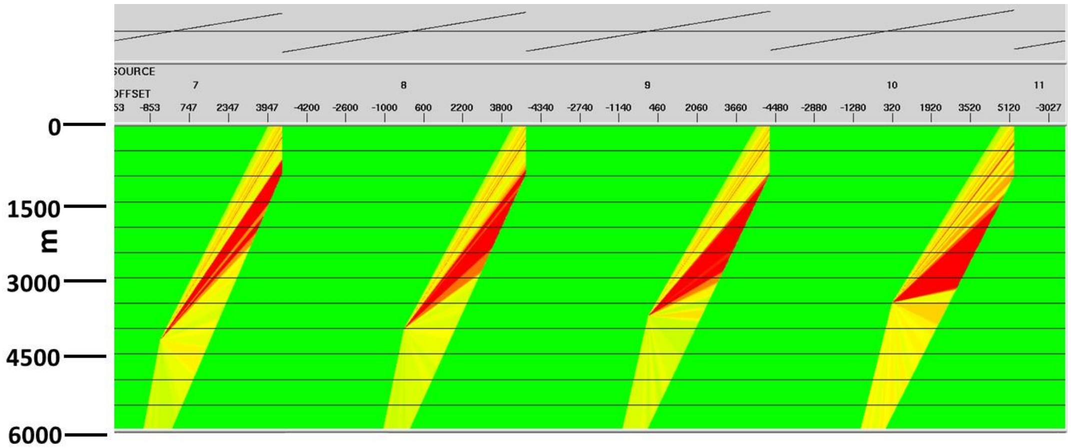

FIG. 11. Source beams with linear offset-dependent shifts applied to affect beam rotation.

We have separated the rotation and alignment processes for shadow beam gathers into four separate operations which compute and apply static shifts to the individual traces within the source beam gathers;

- A rotation static, which depends linearly on source index and linearly on the 'source-receiver offset'. r_stat = (S-index*A*offset), where S-index is the source index, adjusted for zero rotation position, and A is an adjustable scalar.

- A position adjustment static, which corrects for position drift induced by the rotation static; it is quadratically dependent on source index. p_stat = (S-index**2)*B + C, where S-index is the adjusted source index, B is an adjustable scalar, and C is an adjustable constant.

- A linear tilt static, linearly dependent upon source index, which corrects for positional trends induced by the rotational static and positional static. l_stat = (S-index*D) + E, where D is a scalar controlling tilt and E is an adjustable bias.

- A trim static, currently quadratically dependent upon source index, which is applied only over a limited range of source index to further align the beam gathers. t_stat = (S-index**2)*F, where F is an adjustable scalar

We currently have no deterministic theory guiding our selection of the particular parameters or formulas for the trace statics described above. It is mostly a 'Monte Carlo' process of trial and error. The size of the scalar A is adjusted to give 360deg of rotation over the collection of 35 beam gathers. Figure 12 displays the set of 35 gathers with the rotation static applied. Comparing the projected beams in each gather, we can see that the incremental rotations are distributed over the entire 360deg.

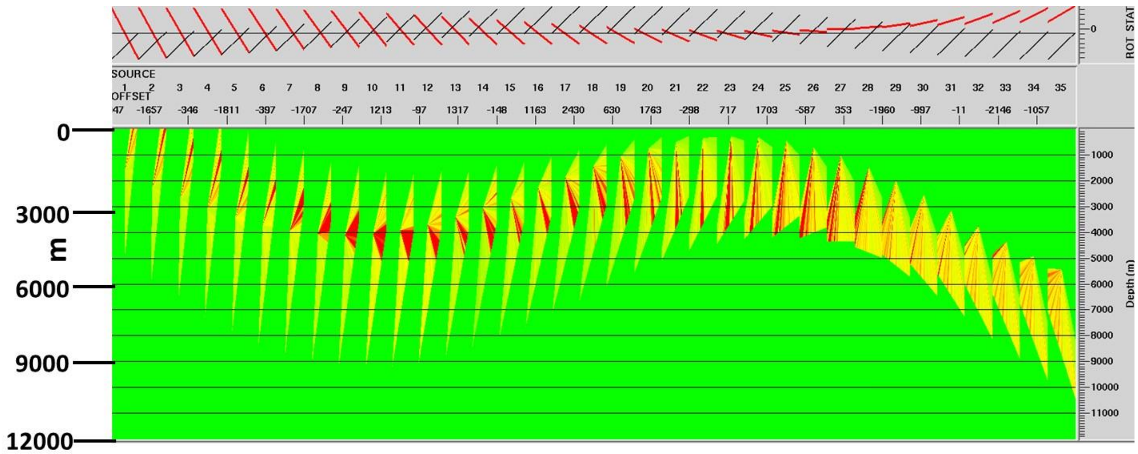

FIG. 12. Source gathers with source points adjusted to source positions around acquisition circle, rotation statics applied to rotate beams. Application of offset-dependent rotation leaves a residual that appears to be roughly quadratic in source position. Header plot: black is source-receiver offset, red is offset-dependent rotation.

We can also see that the deviations of the beam gather origins appear roughly quadratic in form, hence the quadratic formula used for the position static. When we estimate B and C, we improve the fit of the beam gather origins to linearity, as shown in Figure 13.

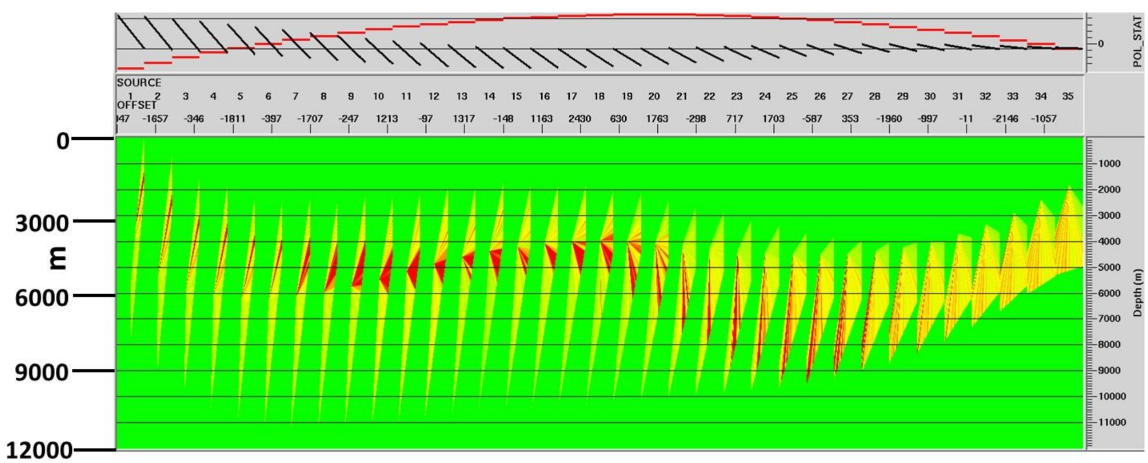

FIG.13. Source beam gathers with sources positioned around circumference of acquisition circle, beams rotated by rotation statics, positions compensated by quadratic position statics. Header plot: red is quadratic source position adjustment.

Estimating values of D and E for the linear static, we can improve the fit even further, as in Figure 14, where only a few beam-gather origins deviate from linearity. By estimating a trim static scalar, F, to be applied only over the gathers whose origins deviate from linearity, we can improve the fit further, as shown in Figure 15.

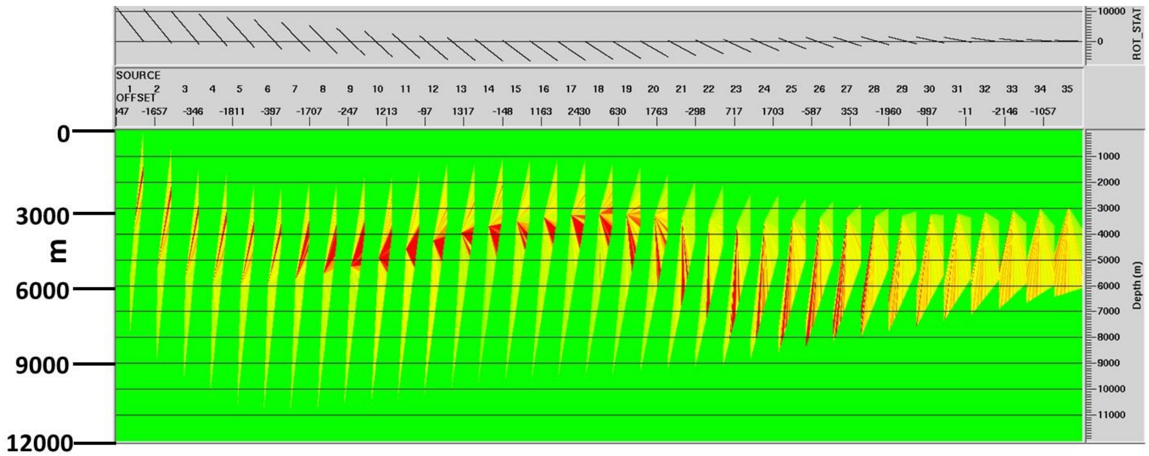

FIG. 14. Source beam gathers, sources positioned around circumference of acquisition circle, beams rotated with rotation statics, quadratic position statics applied to adjust, trim statics applied for further alignment.

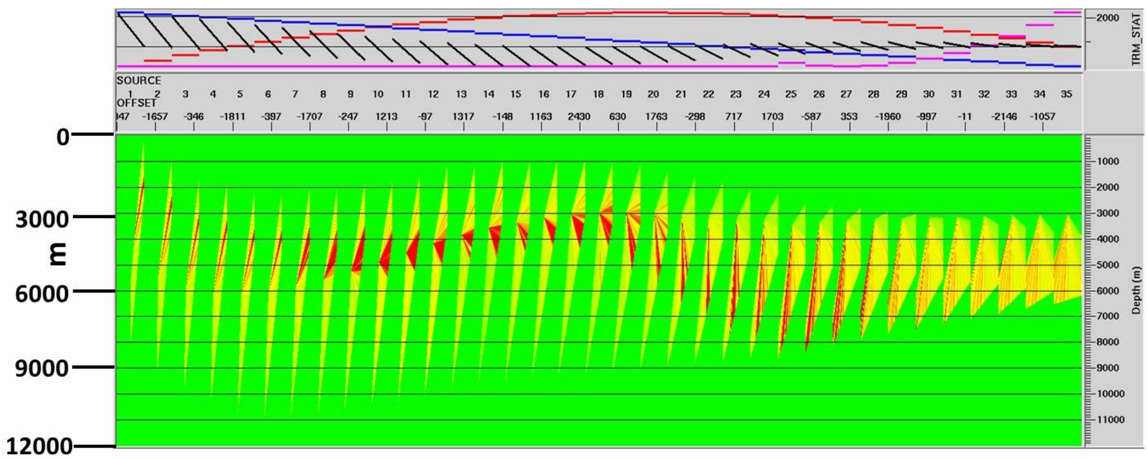

FIG. 15. Source beam gathers with all position, rotation, trim and adjustment statics applied.

Stacking the beam gathers

With the beam gathers corrected by rotation and time shifts to align their apertures for stacking, we access the gathers by source number and another trace header by which the individual traces can be identified—in this case, we chose the ‘source-receiver offset’, which is artificial for these gathers in any case. When we read the ensemble of corrected source gathers using these identifiers and stack by common source-receiver offset, we get an image shown in Figure 16. In this figure, we have superimposed the circular aperture whose interior we are trying to image. Given the uncertainty of our admittedly ad hoc corrections applied to the source beam gathers, we consider the image in Figure 16 to be a proof of principal, rather than a final result.

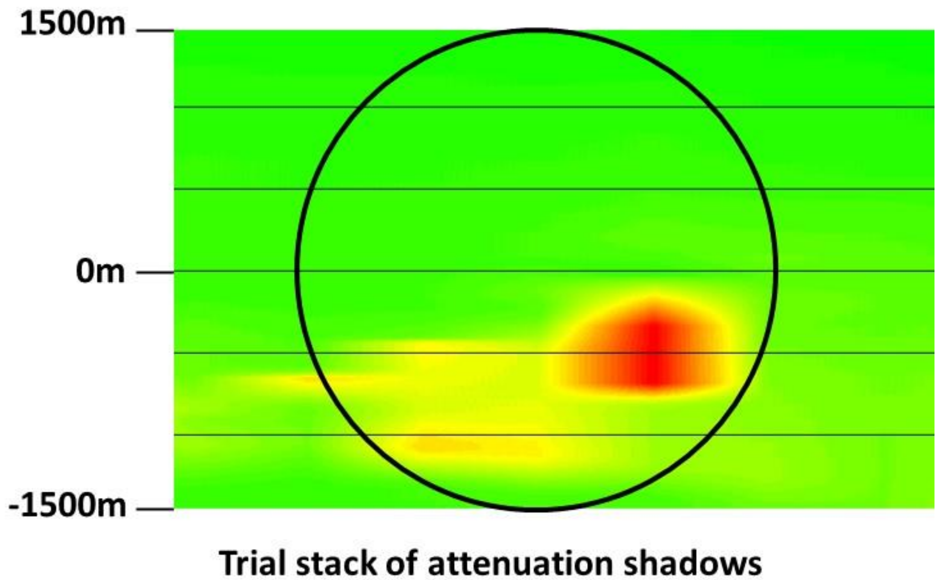

Fig. 16. Stack over image space coordinates of the 35 source shadow beams after position, rotation, and adjustment statis applied.

DISCUSSION

What we have demonstrated in this research is an unconventional approach to attenuation tomography, which involves no picking of waveform arrivals, as required by time-of-flight tomography, thus avoiding the attendant picking errors induced particularly by noisy data. We base our magnitude determination for waveforms on an envelope measurement, which is not especially sensitive to waveform shape, timing, or phase. The inverse of this magnitude is then assigned as the 'shadow strength' for the signal on each trace, and is assigned to every sample on the trace. To centre the envelope measurements on the actual waveform arrivals, each trace is corrected for the travel time along the particular segment represented by its raypath across the circular aperture. In the case of traces passing through an object, the envelope function will be centred on the 'expected' arrival, rather than the actual arrival, which will typically be at an earlier time. Nevertheless, we accept the envelope value of this 'expected' arrival as a measure of the amplitude of the energy transmitted through the object.

Strictly speaking, the rotations which we apply to the beam gathers after the inverse RT transform should be performed with matrix rotations, but we adopted the linear offset-dependent time shift as a quick and easy alternative to demonstrate proof of principle. Likewise, the source and offset-dependent time shifts applied to further correct the positioning and orientation of the shadow beam gathers were determined in an ad hoc manner and presently have no clear mathematical justification.

It is also unclear what coordinates should be assigned to the beam gather traces to stack them over common image coordinates. As well, it may be that the trace amplitudes of the beam gathers should be multiplied by the inverse travel distance, as shown in Figure 17, because amplitude scaling within the inverse RT transform is not considered. Both these questions need to be explored further.

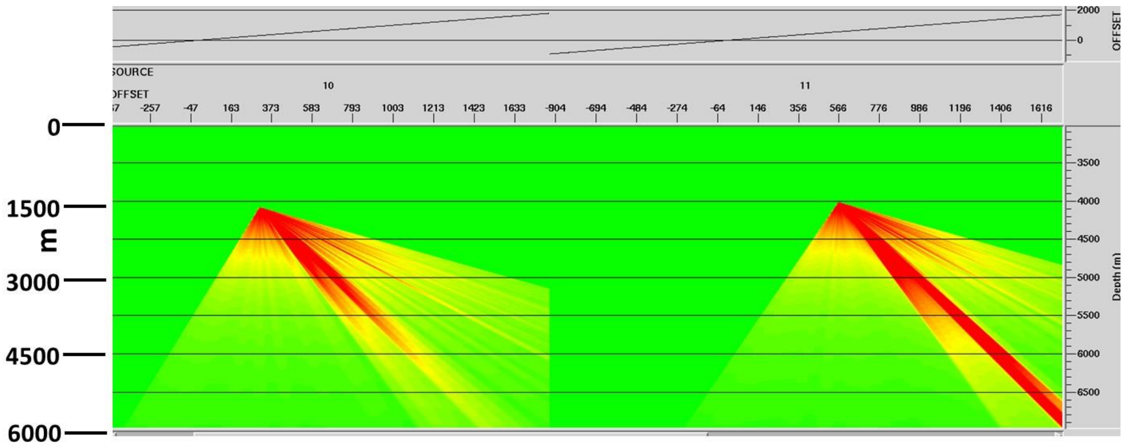

FIG.17. Two beam gathers showing attenuation due to travel distance—this has NOT been applied to the work described above.

CONCLUSIONS

Our goal in this research has been to develop a method for detecting and outlining objects immersed in a circular array of transducers, to provide a starting model for Full Waveform Inversion. The acquisition geometry appears to be ideal for application of traditional travel-time tomography, which has been explored by. In our research, we first explored an unconventional approach related to travel-time tomography (Henley, 2021), which relied (as does tomography) on picked first arrivals of transmitted waveforms. While we showed some interesting results, we decided to alter our approach to look at amplitude attenuation instead of arrival times, bypassing the always-troublesome process of event picking. By using some credible but hand-waving arguments, we have been able to convert the original source gathers of the circular acquisition into shadow beam gathers, and to demonstrate the manipulation and ultimate stacking of these gathers to yield a 'shadow stack' or attenuation image of the surveyed circular space. We contend that the image, shown in Figure 16 is a representation of the rough shape and position of the object within the circular aperture of the survey. The advantages of the demonstrated method compared to earlier results is that no arrival picking is required, and the envelope computation involved is much less sensitive to noise than any picking process.

As outlined in the Discussion, we need to revisit several aspects of the procedure we have outlined above, to make them more theoretically defensible and easier to use on a routine basis.

ACKNOWLEDGEMENTS

The author acknowledges the support of CREWES and its sponsors, as well as NSERC, and discussions with CREWES staff

REFERENCES

Henley, D. C., 1999, Radial trace computational algorithms at CREWES: CREWES Research Report, **11**, 35, 12.

Henley, D. C., 2003, Coherent noise attenuation in the radial trace domain, Geophysics, **68**, No. 4, 1408-1416.

Henley, D. C., and Wong, J., 2019, Let there be light: illuminating physical models from the surface: *CREWES Research Report*, **31**, 22, 27.

Henley, D. C., 2020, A tale of two realities; reconciling physical and numerical modeling via 'bootstrap' processing: CREWES Research Report, 32, 23, 28.

Henley, D. C., 2021, Preliminary processing of physical modeling data from circular arrays: *CREWES Research Report*, **33**, 15, 17.

Margrave, G. F., Lamoureux, M. P., and Henley, D. C., 2011, Gabor deconvolution: estimating reflectivity by nonstationary deconvolution of seismic data, Geophysics, **76,** No. 3, pp W15-W30.

Romahn, S. J., and Innanen, K. A., 2017, The seismic physical modelling laboratory as a tool for design and appraisal of FWI methods: *CREWES Research Report*, **29**, 66, 22.

Wong, J., Mahmoudian, F., Gallant, E. V., and Bertram, M. B., 2010, Seismic physical modeling measurements on solid surfaces: *CREWES Research Report*, **22**, 89, 11.

Wong, J., Bertram, K. L., and Hall, K. W., 2015, Upgrading the CREWES Seismic Physical Modeling Facility: *CREWES Research Report*, **27**, 74, 11.

Wong, J., Zhang, H., Kazemi, N., Bertram, K. L., Innanen, K. A., and Shor, R., 2019, Physical modeling of seismic illumination and SWD: *CREWES Research Report*, **31**, 53, 14.

Wong, J., Bertram, K. L., Zhang, H., Hall, K. W., and Innanen, K. A., 2020, Enhanced source hardware and tank for physical modelling: *CREWES Research Report*, **32**, 55, 24.